Finite Time Horizon Analysis of Launch Vehicles Under Mass and Thrust Uncertainty ⋆

Felix Biertümpfel * **Samir Bennani** ** **Harald Pfifer** *

* *University of Nottingham, Faculty of Engineering, NG7 2RD, Nottingham,
United Kingdom (e-mail: felix.biertumpfel@ nottingham.ac.uk,
harald.pfifer@nottingham.ac.uk)*
** *ESTEC, ESA, 2201AZ, Noordwijk, Netherlands (e-mail:
samir.bennani@esa.int)*

Abstract: This paper presents a new approach to include thrust and mass uncertainties in the worst case loads analysis of launch vehicles during the atmospheric ascend. The analysis is based on recent results on the worst case gain computation of uncertain, finite time horizon linear time varying (LTV) systems. Representing the uncertainties as integral quadratic constraints, the worst case gain condition can be formulated as a parameterized Riccati differential equation (RDE). While this framework allows including certain parametric uncertainties, e.g., aerodynamic uncertainties, it is not straightforward to include thrust uncertainty in the launcher analysis. The reason being that there is an inherent coupling between the thrust and the mass of the launcher, such that any uncertainty in the thrust also effects the mass of the launcher. Further, both thrust and mass have a direct effect on the launch trajectory, whereas the LTV model is obtained via linearization along the nominal trajectory. Hence, it is no longer valid, for large perturbations of the launch trajectory. The former issue is resolved in the paper by including a mass state in the launcher model and treating the thrust uncertainty as an external disturbance. For the latter problem it is proposed to cover a set of launch trajectories with a dynamic uncertainty. Using the robust LTV framework, a worst case aerodynamic loads analysis under thrust uncertainty and wind disturbances is performed in this paper. The results are compared to a Monte Carlo simulation on a high fidelity nonlinear launcher model.

Keywords: Robustness Analysis, Uncertain Linear Systems, Space Vehicles

1. INTRODUCTION

A significant amount of time in the pre-launch preparation of expandable launch vehicles (ELVs) is spend on the optimization of the ascent trajectory and the respective tuning of the launcher's controller. One of the main optimization objectives is the reduction of the maximal aerodynamic loads on the launcher due to wind disturbance. Until hours before launch, updates are made using on day wind data gathered by wind-balloons etc., to identify a load minimizing trajectory based on gravity turns (Dukeman and Hill (2008)). Still, there is no guarantee that the actual wind profile and/ or the launcher's parameters accurately match the assumed values of the these calculations. Besides wind disturbances, especially deviations in the launchers thrust and mass have a significant influence on the actual trajectory and consequently the occurring aerodynamic loads.

The state of the art approaches to analyze the influence of the expected perturbation/ uncertainty set are Monte Carlo analyses and worst case optimizations conducted on the nonlinear model of the ELV (Hanson and Beard (2012)). While these methods can work directly with the high fidelity nonlinear model, their main disadvantage is the high computational effort. They also only provide a lower bound of the worst case aerodynamic load. Therefore, a linear worst case analysis for aerodynamic loads considering wind disturbances and thrust/mass perturbations is

proposed in this paper. It complements a nonlinear Monte Carlo simulation by providing a strict upper bound.

In Biertümpfel et al. (2019), an approach for a finite horizon linear time varying (LTV) worst case loads analysis of launch vehicles is presented. It is based on the recent extension of the bounded real lemma (BRL) for LTV systems to integral quadratic constraints (IQCs) in Seiler et al. (2019) and a corresponding worst case gain optimization framework in Biertümpfel and Pfifer (2018). The latter allows for an efficient analysis of industry-sized LTV systems under a variety of perturbations, such as parametric uncertainty, saturations or time delays. The proposed analysis in Biertümpfel et al. (2019) respects the ELV's time changing dynamics and covers realistic wind turbulence. Thus, it allows for the calculation of an valid upper for the respective nonlinear analysis. However, the analysis is limited to uncertainties which do not noticeably effect the launch trajectory. This implicitly excludes thrust and mass uncertainties as these result in a continuous drift from the design trajectory. Thrust uncertainties are in linear analysis literature, see e.g. Simplicio et al. (2016), often only treated as an uncertainty on the thrust vector control. They do not account for the coupling of mass and thrust, neither for the deviation from the launch trajectory.

To account for these short comings, in this paper the launcher's dynamics are linearized along the nominal trajectory treating the thrust as an external input and the mass as a state. Consequently, a variation from the nominal thrust in the LTV model

results in a accurate description of the deviation from the reference trajectory. As the mass and the thrust of the launcher are directly connected by the exhaust mass flow, the LTV representation of the ELV inherits this coupling. Finally, a dynamic uncertainty with time varying weight is used to cover the changing dynamics when deviating from the linearized trajectory.

As the analysis framework is based on a dissipation inequality the worst case disturbance signal is only bounded in its $L_{2[0,T]}$ norm (Green and Limebeer (1995)). Thus, an appropriate scaling and filtering of the disturbance inputs is necessary to restrict the analysis to realistic disturbance inputs. In case of the wind disturbance signal, the approach in Biertümpfel et al. (2019) is used. It applies a time varying Dryden filter in connection with a gain and high pass filter to shape the worst case inputs into wind disturbances representative of Dryden-like turbulence. The thrust disturbance is scaled using the $L_{2[0,T]}$ norm of the thrust uncertainty analyzed in the nonlinear simulation. This guarantees that the worst case analysis covers the maximal allowable disturbance of the nonlinear system due to a variation in thrust norm-wise.

The paper contributes an approach to analyze coupled thrust and mass uncertainties in the linear worst case loads analysis of a launch vehicle under wind disturbance. It incorporates the thrust perturbation as an adequately scaled input disturbances which is directly coupled with the mass of the ELV in Section 3.4. Contrary to commonly used parametric uncertainties, this allows to consider the perturbations' effects on the trajectory and states in the LTV analysis as shown in Section 3.3. The respective perturbed trajectories/dynamics are covered by a weighted dynamic output uncertainty in Section 3.6. The applicability of the approach is demonstrated by a comparison to the results of an random search conducted on the nonlinear model of the launcher in Section 4.

2. BACKGROUND

2.1 Integral Quadratic Constraints

IQCs are used to bound the input/output behavior of an uncertainty Δ. The time domain definition of an IQC is based on a filter $\Psi \in \mathbb{RH}_\infty^{n_z \times (n_v + n_w)}$ and a $n_z \times n_z$ real, symmetric matrix M (Pfifer and Seiler (2016)). The uncertainty Δ satisfies the IQC defined by M and Ψ if the output z of the filter Ψ fulfills the quadratic time constraint

$$\int_0^T z(t)^T M z(t)\, dt \geq 0 \qquad (1)$$

for all $v \in L_2[0,T]$ and $w = \Delta(v)$ over the interval $[0,T]$. In this case the short notation $\Delta \in IQC(\Psi, M)$ is used. Furthermore, $L_2[0,T]$ denotes a L_2 measurable signal (Green and Limebeer (1995)).

2.2 Robust Performance Analysis of LTV systems

Based on the worst case analysis condition of nominal LTV systems in Green and Limebeer (1995) and the time domain IQC representation of the uncertainty Δ, a robust performance analysis can be proposed (Biertümpfel and Pfifer (2018); Seiler et al. (2019)). The problem addresses the interconnection of a known LTV system G_t and a perturbation Δ. The perturbation is assumed to satisfy an IQC described by (Ψ, M), i.e. $\Delta \in IQC(\Psi, M)$. In this case, the IQC filter Ψ can be introduced in the interconnection as shown in Fig. 1. The dynamics of the interconnection depend on an extended LTV system G_{ext} of the following form:
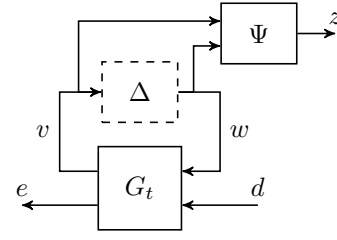

Fig. 1. Feedback Interconnection LTV system G_t and uncertainty Δ

$$\dot{x}(t) = A(t)\, x(t) + \begin{bmatrix} B_1(t) & B_2(t) \end{bmatrix} \begin{bmatrix} w(t) \\ d(t) \end{bmatrix}$$

$$\begin{bmatrix} z(t) \\ e(t) \end{bmatrix} = \begin{bmatrix} C_1(t) \\ C_2(t) \end{bmatrix} x(t) + \begin{bmatrix} D_{11}(t) & D_{12}(t) \\ D_{21}(t) & D_{22}(t) \end{bmatrix} \begin{bmatrix} w(t) \\ d(t) \end{bmatrix}. \qquad (2)$$

In (2), $x(t) \in \mathbb{R}^{n_x}$ represents the state vector containing the states of G_t and Ψ, $d(t) \in \mathbb{R}^{n_d}$ the input vector and $e(t) \in \mathbb{R}^{n_e}$ the output vector. The time domain inequality (1) enforced on the output z of Ψ is used to replace the explicit representation of the uncertainty $w = \Delta(v)$.

The finite horizon worst case $L_2[0,T]$ to $\|e(T)\|_2$ gain is then defined as follows:

$$\|F_u(G_t, \Delta)\|_2 := \sup_{\substack{\Delta \in IQC(\Psi, M)}} \sup_{\substack{d \in L_2[0,T] \\ d \neq 0, x(0) = 0}} \frac{\|e(T)\|_2}{\|d(t)\|_{2[0,T]}}. \qquad (3)$$

Geometrically interpreted, it describes the ball upper bounding the worst case output $e(T)$ at the terminal time T over all $\Delta \in IQC(\Psi, M)$ for $\|d(t)\|_{2[0,T]} = 1$, with

$$\|d(t)\|_{2[0,T]} = \sqrt{\int_0^T d^T(t)d(t)dt}. \qquad (4)$$

A dissipation inequality can be formulated to bound the worst case $L_2[0,T]$ to $\|e(T)\|_2$ gain of the interconnection $F_u(G_t, \Delta)$ using the extended LTV system G_{ext} (2) and the finite horizon time domain IQC formulation (1), see Seiler et al. (2019) and Biertümpfel and Pfifer (2018). The dissipation inequality is expressed as an equivalend RDE formulation in the following Theorem:

Theorem 1. Let $F_u(G_t, \Delta)$ be well posed $\forall \Delta \in IQC(\Psi, M)$, then $\|F_u(G_t, \Delta)\|_2 < \gamma$ if there exists a continuously differentiable symmetric $P : [0,T] \to \mathbb{R}^{n_x \times n_x}$ such that

$$P(T) = \frac{1}{\gamma} C_2(T)^T C_2(T), \qquad (5)$$

$$\dot{P} = Q + P\tilde{A} + \tilde{A}^T P - PSP \qquad \forall t \in [0,T], \qquad (6)$$

and

$$R = \begin{bmatrix} D_{11}^T M D_{11} & D_{11}^T M D_{12} \\ D_{12}^T M D_{11} & D_{12}^T M D_{12} - \gamma I \end{bmatrix} < 0 \, \forall\, t \in [0,T], \qquad (7)$$

with

$$\tilde{A} = \begin{bmatrix} B_1 & B_2 \end{bmatrix} R^{-1} \begin{bmatrix} (C_1^T M D_{11})^T \\ (C_1^T M D_{12})^T \end{bmatrix} - A, \qquad (8)$$

$$S = -\begin{bmatrix} B_1 & B_2 \end{bmatrix} R^{-1} \begin{bmatrix} B_1^T \\ B_2^T \end{bmatrix} \qquad (9)$$

and

$$Q = -C_1^T M C_1 + \begin{bmatrix} (C_1^T M D_{11})^T \\ (C_1^T M D_{12})^T \end{bmatrix}^T R^{-1} \begin{bmatrix} (C_1^T M D_{11})^T \\ (C_1^T M D_{12})^T \end{bmatrix}. \qquad (10)$$

Proof. The proof is based on the definition of a time-dependent quadratic storage function $V(x,t) = x^T P(t)x$. After perturbing (6) the resulting Riccati differential inequality can be rewritten as an LMI applying the Schur complement. Multiplying $[x^T, w^T, d^T]$ and $[x^T, w^T, d^T]^T$ on the left and right

side respectively of the LMI results in a dissipation inequality. Integration from 0 to T for zero initial conditions gives

$$\int_0^T z(t)^T M z(t) dt - \gamma \int_0^T d(t)^T d(t) dt \qquad (11)$$
$$+ x(T)^T P(T) x(T) < 0.$$

Equality (5) is perturbed and left and right multiplied with $x(T)^T$ and $x(T)$ respectively resulting in

$$x(T)^T P(T) x(T) - \frac{1}{\gamma} e(T)^T e(T) > 0. \qquad (12)$$

Substituting (11) in (12) and applying the vector 2-norm (Euclidean) $\|e(T)\|_2^2 = e(T)^T e(T)$ results in the upper bound on γ given by (3). ∎

Note that a detailed proof can be found in Seiler et al. (2019). Typically, there exists an infinite number of IQCs to describe a given Δ. In literature (Pfifer and Seiler (2016); Veenman et al. (2016)), it is common praxis to fix Ψ and parameterize M, i.e. M lies within a feasible set $\mathcal{M}$ such that $\Delta \in IQC(\Psi, M)$ for all $M \in \mathcal{M}$. Using this approach, Theorem 1 describes a parameterized RDE. A nonlinear optimization problem can then be formulated to minimize γ:

$$\min_{M \in \mathcal{M}} \gamma$$
$$\text{such that } \forall t \in [0, T]$$

$$P(T) = \frac{1}{\gamma} C_2(T)^T C_2(T)$$
$$\dot{P} = Q + P\tilde{A} + \tilde{A}^T P - PSP \qquad (13)$$
$$R < 0$$

In Biertümpfel and Pfifer (2018) an algorithm to efficiently solve the optimization problem is given. It essentially performs a bisection of γ for a fixed M in an inner loop. In an outer loop a global optimization over M is then performed to find a minimum of γ.

3. LAUNCHER MODEL

3.1 Nonlinear Dynamics

The investigated ELV is built of 3 solid rocket motor stages and an upper module with liquid propulsion. For the analysis the flight segment from $25s$ to $95s$ after lift-off is considered, which is propelled by a solid rocket motor. During this flight phase, the launcher can be assumed symmetrical. Thus, the yaw and pitch dynamics are identical and can be treated as fully decoupled. Hence, it is sufficient to only study the pitch motion of the ELV. Due to the duration and velocity of the flight segment the earth can be assumed flat and non-rotating (Greensite (1967)). Finally, the launcher is treated as a rigid body in this paper, i.e. the influence of propellant sloshing or inertias of the thrust vector control (TVC) are neglected. Given the launcher's configuration, sloshing is not critical during the first stage flight, because of the neglectable fraction of liquids in the overall mass. The launchers dynamics are illustrated in Fig. 2. A formulation in a body fixed coordinate system denoted by the subscript b fixed to the center of gravity (G) is used to formulate the nonlinear equations of motion (EoM). The x_b axis is aligned with the symmetry axis of the launcher and is defined positive in direction of forward travel. The z_b axis is pointing downward building a right hand system with the y_b axis pointing out of the page. The nonlinear EoM are defined as
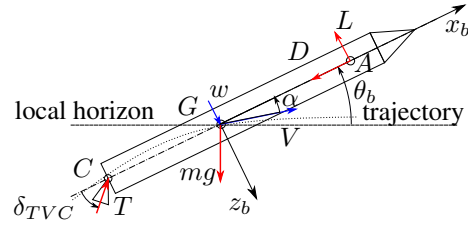

Fig. 2. Expandable launch vehicle in body fixed reference frame

$$\ddot{\theta}_b = \frac{L l_{GA}}{J_y} - \frac{T l_{CG}}{J_y} \sin(\delta_{TVC})$$
$$\ddot{x}_b = \frac{T \cos(\delta_{TVC}) - D}{m} - g_0 \sin\theta_b - \dot{\theta}_b \dot{z}_b \qquad (14)$$
$$\ddot{z}_b = -\frac{L}{m} - \frac{T}{m} \sin\delta_{TVC} + g_0 \cos\theta_b + \dot{\theta}_b \dot{x}_b.$$

In (14), θ_b is the pitch angle of the launcher describing the angle between the body axis and the local horizon. The forward and downward accelerations are denoted by $\ddot{x}_b$ and $\ddot{z}_b$ respectively. V is the velocity of the ELV. L denotes the aerodynamic lift. It is defined positive in upward direction parallel to the z_b axis. The aerodynamic drag D is defined in the same way with respect to the x_b axis. The aerodynamic center A describes the point of attack of L as well as D. Both aerodynamic forces are a function of the angle of attack α defined as

$$\alpha \approx \frac{\dot{z}_b - w}{\dot{x}_b}, \qquad (15)$$

where w denotes the (external) wind disturbance in z_b direction. The thrust T acts at the nozzle reference point C. It can be deflected by the angle δ_{TVC} using the thrust vector control. Due to the characteristics of the solid rocket motor, the thrust is not controllable. It is defined by

$$T(t) = v_{ex}(t) \dot{m}_{ex}(t), \qquad (16)$$

where v_{ex} is the exhaust velocity and $\dot{m}_{ex}$ the exhaust mass flow of the engine. As a consequence of perturbations in the combustion process as well as tolerances in the packing process, T has some degree of uncertainty. Based on post-flight analysis of mission data, a common assumption is a constant thrust uncertainty of up to $\pm 10\%$. The thrust profile (16) directly relates to the launcher mass m by m_{ex}. The mass of the launcher is given by

$$m(t) = m_0 - \int_0^{T_f} \dot{m}_{ex} dt = m_0 - \int_0^{T_f} \frac{T(t)}{v_{ex}(t)} dt. \qquad (17)$$

It is assumed that the thrust uncertainty is purely a consequence of $\dot{m}_{ex}$ and not v_{ex}. An uncertainty in T directly effects the mass (17), but also directly and indirectly through m effects the attitude and translation of the launcher (14). J_y denotes the overall mass moment of inertia with respect to G. As the influence on the trajectory is neglectable, J_y is treated as decoupled from thrust and mass. The lever arms of the introduced forces result in a angular momentum around C are l_{CG} and l_{GA} defined as absolute distances between C and G, and G and A respectively. Launching from a location close to the equator the altitude dependent gravitational acceleration $g_0(h)$ is calculated based on the world geodetic system 84 (WGS 84).

3.2 Trajectory Calculation

To minimize the static aerodynamic loads and maximizing the longitudinal acceleration for the given amount of fuel, the launcher performs a so called gravity turn maneuver (Wiesel

(2010)). Under the assumption that the centrifugal and the gravitational force on the launcher compensate each other, the initial value problem

$$\dot{h} = V \sin\theta_b \qquad\qquad \dot{X} = V \cos\theta_b$$
$$\dot{V} = \frac{T-D}{m} - g\sin\theta_b \qquad \dot{\theta}_b = -\frac{g}{V}\cos\theta_b \qquad (18)$$

is derived from the launcher's EoMs (14). In (18), h is the altitude and X is the downrange distance. Solving (18) for a given h_0, θ_0, V_0 and X_0 provides a pitch program for the launcher, which results in $\alpha \approx 0$ and $\delta_{TVC} \approx 0$ during the ascent. In case of perturbations of T, the equilibrium of gravitational and centrifugal force underlying (18) is not longer fulfilled, if the pre-calculated pitch program is followed. This results in a build up of $Q\alpha$ and a continuous deviation from the design trajectory.

3.3 Linear Dynamics

The LTV worst case analysis of the ELV requires a linear representation of the ELV along the calculated gravity turn trajectory. Thus, the nonlinear dynamics in (14) are linearized along the trajectory. This results in a finite horizon LTV system G_t:

$$\dot{x}_t(t) = A_t(t)\,x_t(t) + B_t(t)\,d(t)$$
$$e(t) = C_t(t)\,x_t(t) + D_t(t)\,d(t), \qquad (19)$$

where $x_t(t) \in \mathbb{R}^{n_x}$ represents the state vector, $d(t) \in \mathbb{R}^{n_d}$ the input vector and $e(t) \in \mathbb{R}^{n_e}$ the output vector. Given (14), the state vector is $x_t = [\Delta\theta_b, \Delta\dot{\theta}_b, \Delta\dot{z}_b, \Delta\dot{x}_b, \Delta m]^T$, the input vector is $d = [\Delta\delta_{TVC}, \Delta w, \Delta T]^T$ and the output vector $e = [\Delta\theta_b, \Delta Q\alpha]^T$. Here, Δ refers to the deviation from the reference value on the design trajectory, it will be dropped in the following to shorten the notation. $Q\alpha$ is a measure for the static aerodynamic load and defined as the product of dynamic pressure Q and angel of attack α. The system matrices A_t, B_t, C_t and D_t are:

$$A_t = \begin{bmatrix} 0 & 1 & 0 & 0 & 0 \\ 0 & -\frac{J_{y,0}}{J_{y,0}} & \frac{L_0 l_{GA,0}}{\dot{x}_{b,0} J_{y,0}} & 0 & 0 \\ -g_0\sin\theta_{b,0} & -\dot{x}_{b,0} & \frac{L_0}{\dot{x}_{b,0}m_0} & \dot{\theta}_{b,0} & 0 \\ -g_0\cos\theta_{b,0} & 0 & -\dot{\theta}_{b,0} & 0 & -\frac{T_0-D_0}{m_0^2} \\ 0 & 0 & 0 & 0 & 0 \end{bmatrix}, \qquad (20)$$

$$B_t = \begin{bmatrix} 0 & 0 & 0 \\ -\frac{T_0 l_{CG,0}}{J_{y,0}} & -\frac{L_0 l_{GA,0}}{\dot{x}_{b,0} J_{y,0}} & 0 \\ -\frac{T_0}{J_{y,0}} & -\frac{L_0}{\dot{x}_{b,0}m_0} & 0 \\ 0 & 0 & \frac{1}{m_0} \\ 0 & 0 & -\frac{1}{v_{ex,0}} \end{bmatrix}, \qquad (21)$$

$$C_t = \begin{bmatrix} 1 & 0 & 0 & 0 & 0 \\ 0 & 0 & \frac{Q_0}{\dot{x}_{b,0}} & 0 & 0 \end{bmatrix} \qquad (22)$$

and

$$D_t = \begin{bmatrix} 0 & 0 & 0 \\ 0 & -\frac{Q_0}{\dot{x}_{b,0}} & 0 \end{bmatrix}. \qquad (23)$$

All coefficients in (20)-(23) are strictly time dependent, which is omitted only to shorten the notation. The subscript 0 relates to the reference value on the nominal trajectory.

The common approach in literature is to treat thrust and mass as parameters in the linearization, e.g. Simplicio et al. (2016). Thus, a thrust and mass perturbation can only be respected in the linear analysis by treating the respective reference values T_0 and m_0 in the system matrices as uncertain. Consequentially, the direct and indirect influence of a thrust perturbation on the launcher's states as in (14) is not covered, but only its

influence on the controllability via δ_{TVC}. In this paper, the thrust is defined as an input and the mass as a state in the linearization. Therefore, the LTV model retains the inherent coupling between thrust and mass disturbance as consequence of (16) and (17). If the thrust input is adequately scaled, it can accurately represent a thrust uncertainty in the nonlinear dynamics. Hence, the LTV description of the launcher in (19) presents a more accurate approximation of the ELV's nonlinear dynamics (14) for the worst case analysis than the standard literature approaches.

3.4 Modeling Uncertainty Effects as External Disturbance

Applying the strict BRL, the search space for the worst case disturbance signals is only restricted by the $L_{2[0,T]}$ norm, $\|d(t)_{WC}\|_{2[0,T]} = 1$. To get meaningful results, the thrust input needs to be scaled to represent a 10% thrust uncertainty in the nonlinear dynamics. A reasonable scaling is the $L_{2[0,T]}$ norm of 10% nominal thrust for the given analysis horizon, i.e. $k_T = \|0.1T_0(t)\|_{2[0,T]}$. Thus, the LTV analysis covers the maximal thrust disturbance considered in the nonlinear analysis norm-wise. Consequentially, the LTV worst case analysis also presents an upper bound to the respective constant thrust disturbance, as the latter's norm is worst case re-distributed. However, this can lead to a worst case thrust disturbance which exceeds $\pm10\%$ locally. This is acceptable as it only leads to an additional conservatism of the LTV analysis whose main intend is to provide a reliable upper bound for the nonlinear analysis. Additional conservatism can even be considered beneficial, taking into consideration that the information about the actual thrust disturbance during the launch is very limited.

3.5 Wind Disturbance Model

The analyzed wind disturbance w shall resemble Dryden turbulence profiles, which are frequently used in aerospace certification (Hoblit (1988)). In the nonlinear analysis the Dryden filter G_w for vertical turbulence

$$\dot{x}_w(t) = \begin{bmatrix} 0 & 1 \\ -\left(\frac{V(t)}{L_w(h)}\right)^2 & -2\frac{V(t)}{L_w(h)} \end{bmatrix} x_w(t) + \begin{bmatrix} 0 \\ \left(\frac{V(h)}{L(h)}\right)^2 \end{bmatrix} n_w(t)$$
$$w(t) = \begin{bmatrix} \sigma(h)\sqrt{\frac{L_w(h)}{\pi V(t)}} & \sigma(h)\frac{L_w(h)}{V(t)}\sqrt{\frac{3L_w(h)}{\pi V(t)}} \end{bmatrix} x_w(t), \qquad (24)$$

with white noise input n_w is implemented to generate w. The white noise signal is generated by Matlab's internal band-limited white noise block. G_w shapes signals with constant power spectral density (PSD) into turbulence profiles statistically matching real turbulence. In (24), V is the velocity of the ELV, σ is the turbulence intensity and L_w is the turbulence scale length.

As a consequence of the discussed norm bound on the input disturbance signal imposed by the strict BRL, the Dryden wind filter in (24) cannot directly be implemented in the LTV analysis. In Biertümpfel et al. (2019) a corresponding modification of the Dryden filter is introduced. It consists of a pre-filter and a scaled LTV formulation $G_{w,LTV}$ of (24):

$$\dot{x}_w(t) = \begin{bmatrix} 0 & 1 \\ -\left(\frac{V(t)}{L_w(t)}\right)^2 & -2\frac{V(t)}{L_w(t)} \end{bmatrix} x_w(t) + \begin{bmatrix} 0 \\ \left(\frac{V(t)}{L_w(t)}\right)^2 \end{bmatrix} d_{WC,w}(t)$$
$$v_w(t) = k_{w_i} \begin{bmatrix} \sigma(t)\sqrt{\frac{L_w(t)}{\pi V(t)}} & \sigma(t)\frac{L_w(t)}{V(t)}\sqrt{\frac{3L_w(t)}{\pi V(t)}} \end{bmatrix} x_w(t). \qquad (25)$$

Using $G_{w,LTV}$, the wind disturbance w in the LTV worst case analysis resulting from filtering the norm bounded worst case wind input signal $d_{WC,w}$ by $G_{w,LTV}$ has comparable frequency content and amplitudes as real turbulence.

3.6 Trajectory Uncertainty Model

As described in Section 3.1, a thrust uncertainty has a direct and indirect influence on the nonlinear dynamics in (14). Consequently, a perturbation in the nominal thrust profile leads to a deviation from the design trajectory as (18) no longer holds, which itself influences the nonlinear dynamics. Thus, linearizing the nonlinear dynamics along such a perturbed trajectory results in system matrices different to the ones of the nominal gravity turn in (20)-(23). It is necessary to cover these perturbed dynamics in the LTV worst case analysis. Otherwise, the direct comparison with the nonlinear analysis is of little meaning. The following uncertain LTV representation of the launcher is introduced whose range of behaviors covers the dynamics along the perturbed trajectories.

$$G_{LV} = (1 + W_{LTV}\Delta)G_t \qquad (26)$$

In (26), Δ is a norm bounded dynamic LTI uncertainty, with $\|\Delta\|_\infty \leq 1$ and W_{LTV} is a time varying shaping filter. The weighting filter W_{LTV} is chosen based on the approach proposed in Hindi et al.. LTV models of eight perturbed trajectories spanning a range of $\pm 10\%$ constant thrust uncertainties are generated. At frozen time points, the weighting is calculated such that all perturbed models are included in the uncertainty set (27). Finally, the time varying weighting is obtained by piecewise cubic polynomial interpolation. For example, the nominal dynamics extended with the weighting filter at 40s are shown in comparison with the perturbed dynamics in Fig. 3.
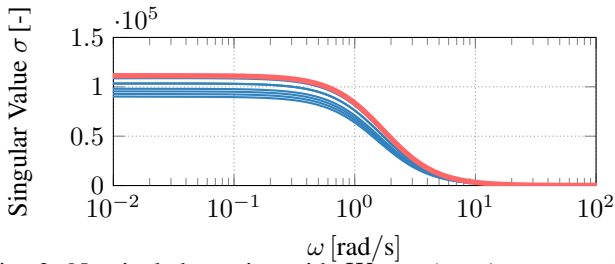

Fig. 3. Nominal dynamics with W_{LTV} (━━) vs. perturbed dynamics (──) at $t = 40$s.

3.7 Augmentation

To track the calculated pitch program and keep the deviation to the nominal trajectory minimal, a feedback controller is necessary. This controller also needs to stabilize the aerodynamically unstable ELV. Therefore, a fixed-gain PID controller C was designed using the dynamics at the point of maximum dynamic pressure $Q_{max} = 5.603 \cdot 10^4$Pa during the ascent. Using loop-shaping, gains were calculated so that a maximum tracking bandwidth of 6rad/s, with $40°$ phase margin and 6dB gain margin is achieved. These margins are in compliance with the recommendations in Greensite (1967). Applying this controller to the nominal launcher, the nonlinear simulation shows sufficient tracking of the pitch program ($|\Delta\theta_b \leq 0.1°|$). Furthermore, the absolute value of the occurring static aerodynamic load $|Q(t)\alpha(t)|$ never exceeds the allowed limit of $2.2 \cdot 10^5$Pa$°$ under the test scenarios proposed by ESA. Further, the following second order dynamics of the TVC are included in the launcher model.

$$G_{TVC}(s) = \frac{1}{0.000374s^2 + 0.0384s + 1} \qquad (27)$$

4. ANALYSIS

4.1 Analysis Interconnection for LTV Worst Case Analysis

The LTV worst case analysis structure is shown in Fig. 4. G_{ELV}
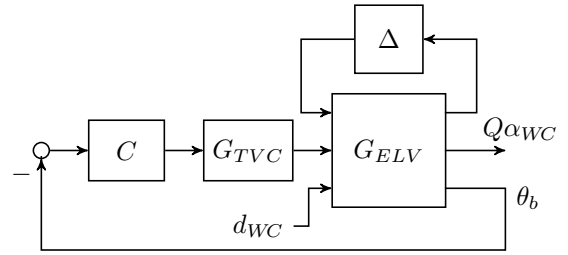

Fig. 4. Launcher interconnection for LTV worst case analysis

represents the launcher's uncertain LTV model G_{LV}, extended with the LTV wind filter $G_{w,LTV}$ and the thrust scaling k_T at the related inputs. The underlying nominal LTV model G_t is computed via numerical linearization over the given analysis horizon $[25s, 95s]$ with a step size of 0.1s. The input $d_{WC} = [d_{WC,w}, d_{WC,T}]^T$ represents the wind and thrust disturbance respectively. The launcher is augmented as introduced in Section 3.7. The LTV worst case aerodynamic load $Q\alpha_{WC}$ is calculated applying the algorithm in Biertümpfel and Pfifer (2018) on the optimization problem (13) originating from Theorem 1. Therefore, the interconnection in Fig. 4 has to be transfered into the IQC framework as described in Section 3.2. The dynamic LTI uncertainty Δ is represented by the conic combination of two IQCs, $IQC_1(\Psi_1, M_1)$ and $IQC_2(\Psi_2, M_2)$ (Pfifer and Seiler (2016)). For the analysis, the fixed factorizations are chosen to $\Psi_1 = I_2$ and $\Psi_2 = \frac{1}{s+1}I_2$ and the respective parameterization M_i is restricted to the set $\mathcal{M} = \{M_i \in diag(\lambda_i, -\lambda_i)|, \lambda \in \mathbb{R} > 0, i = 1, 2\}$.

4.2 LTV Worst Case Aerodynamic Load Calculation

The finite horizon worst case $L_{2[0,T]}$ to $\|e(T)\|_2$ gain can only upper bound $Q\alpha_{WC}$ at the respective terminal time T. Therefore, it is necessary to analyze a set of terminal times covering the trajectory. The following analysis is performed on a interval T_i in $[30s, 95s]$ with a step size of 5s. For this grid the scalings k_{w_i} for $G_{w,LTV}$ are calculated by the procedure in (Biertümpfel et al. (2019)). The corresponding scaling of the thrust input $k_{T,i}$ is calculated as described in Section 3.4 for a constant thrust uncertainty of 10%. The first run of the analysis calculating $Q\alpha_1$ for $T_1 = 30$s is conducted with an user defined initial guess for λ_1 and λ_2. For a time efficient analysis the calculation of the following terminal times T_i uses the optimal solution of the previous terminal time T_{i-1}. This exploits that the optimal solution of consecutive final times T_i and T_{i+1} are relatively close and therefore the optimization converges faster. The absolute and relative tolerance of the optimization are $\epsilon_{rel} = 10^{-4}$ and $\epsilon_{abs} = 10^{-6}$. For the bisection, a tolerances of one magnitude less is chosen.

The results for the worst case $Q\alpha_{WC}$ scaled with the limit load $Q\alpha_{lim} = 2.2 \cdot 10^5Pa°$ are shown in Fig. 5. The scaling with $Q\alpha_{lim}$ allows for an easier evaluation of the worst case load's criticality. The values in-between the calculated grid points are linear interpolated. The maximum $Q\alpha_{WC,max}$ along the analysis grid is around 43% of Q_{lim} at 30s. The values of $Q\alpha_{WC}$ remain in this range up to 35s until they start to gradually decrease to around 23% of Q_{lim} at 45s. Two effects contribute to the high $Q\alpha_{WC}$ in this flight segment. Firstly, the turbulence intensity is higher in this segment as it is inverse proportional with the altitude. This directly leads to high wind induced α disturbances. Secondly, the dynamic pressure increases as the launcher accelerates through the denser part of the atmosphere. This also partially compensates the decreasing turbulence am-

plitudes. Fifty seconds after lift-off $\sigma_w < 0.0001\text{m/s}$ and the wind influence diminishes. By this time, the influence of the thrust disturbance is more significant as the α build-up due to a steadily increasing deviation from the nominal trajectory. This in combination with the increasing dynamic pressure up to $Q_{\max} = 5.603 \cdot 10^4\text{Pa}$ at 52s leads to another growth of $Q\alpha_{WC}$ in the region of 50s to 80s. In the final flight segment, the dynamic pressure decreases significantly due to the thinning atmosphere. Hence, the aerodynamic load reduce. The LTV worst case analysis of the T_i set was completed in 1h10min on a standard PC.

4.3 Nonlinear Aerodynamic Load Calculation

The next step is to validate that the LTV worst case envelope presents a valid and adequate upper bound for the nonlinear simulation of the launcher. Therefore, a Monte Carlo simulation in Matlab Simulink is conducted. The nonlinear analysis interconnection is comparable to Fig. 4. The differences are that G_{ELV} represents the nonlinear dynamics and the classic Dryden filter G_w in (24) with white noise input is used to generate the wind disturbance. Furthermore, the thrust is treated directly as an uncertain parameter. The simulation starts at $t_s = 25\text{s}$ and ends at $t_f = 95\text{s}$ after lift-off. A Monte Carlo simulation requires an adequate sample size of disturbance signals and uncertainty combinations. For the former this is achieved by generating 100000 different white noise signals $n_{w_i}(t)$ using the Simulink internal band-limited white noise block with unique noise seeds s_i. The thrust uncertainty is considered by 8 uniform points to cover $\pm10\%$ uncertainty. Subsequently, every noise signal n_{w_i} is evaluated over the δ_T grid. The highest aerodynamic load of the nonlinear analysis $Q\alpha_{MC} = 4.62 \cdot 10^4\text{Pa}^\circ$ occurs for $\delta_T = -0.1$ at $t = 30.7\text{s}$, which is 21.8% of $Q\alpha_{lim}$. The signal $Q\alpha_{MC}$ is shown in Fig. 5. An envelope covering the peaks of the $Q\alpha$ signals over all $n_{w_i}(t)$ for $|\delta_T| \leq 0.1$ scaled with $Q\alpha_{lim}$ is shown in Fig. 5. It can be seen that the LTV worst case envelope encloses the envelope of the Monte Carlo simulation. Furthermore, both analysis show the same characteristic, i.e. a wind disturbance driven peak in the early flight segment and a thrust disturbance induced peak in the region of Q_{max}. The match of both analyses in the Q_{max} region is better than in the early segment of the flight. This is a consequence of the fact that, the strict BRL also considers non-white noise signals which in combination with $G_{w,LTV}$ result in potentially higher turbulence amplitudes. Due to the decreasing turbulence intensity, this effect diminishes at later times leading to a better match. This also suggests a good approximation of the trajectory deviation using ΔT as disturbance input in combination with a weighted dynamic uncertainty.
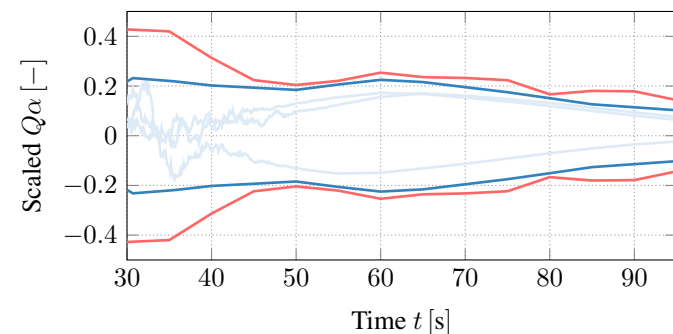

Fig. 5. Analysis results scaled with $Q\alpha_{lim}$: $Q\alpha_{WC}$ bound LTV analysis (———), $Q\alpha_{MC}$ bound Monte Carlo simulation (———), $Q\alpha$ signals Monte Carlo simulation (———)

5. CONCLUSION

The presented LTV worst case loads analysis of an ELV's incorporates the influence of realistic atmospheric disturbance as well as coupled thrust and mass uncertainty. In contrary to common approaches, the thrust uncertainty is respected as an adequately scaled input disturbance rather than a parametric uncertainty in the LTV analysis. Furthermore, the mass is introduced as a state of the LTV model which is directly coupled with the thrust input. This allows not only to respect the thrust's direct influence on the trajectory, but also its indirect influence as a result of the corresponding mass disturbance. Therefore, the LTV model's behavior closely matches the nonlinear model. Extended with a weighted dynamic output uncertainty accounting for the dynamics of perturbed trajectories, the LTV worst case analysis provides an feasible upper bound for the corresponding Monte Carlo simulation. Therefore, the LTV worst case analysis provides a fast and suitable supplement for the certification process of space launchers.

REFERENCES

Biertümpfel, F. and Pfifer, H. (2018). Worst case gain computation of linear time-varying systems over a finite horizon. In *2nd Conference on Control Technology and Applications*.

Biertümpfel, F., Pfifer, H., and Bennani, S. (2019). Finite horizon worst case analysis of launch vehicles. *IFAC-PapersOnLine*, 52(12), 31–36.

Dukeman, G. and Hill, A. (2008). Rapid trajectory optimization for the ARES i launch vehicle. In *AIAA Guidance, Navigation and Control Conference and Exhibit*. American Institute of Aeronautics and Astronautics.

Green, M. and Limebeer, D.J.N. (1995). *Linear Robust Control*. Prentice-Hall, Inc., Upper Saddle River, NJ, USA.

Greensite, A.L. (1967). Analysis and design of space vehicle flight control systems. volume vii - attitude control during launch. Technical report, NASA Marshall Space Flight Center; Huntsville, AL, United States.

Hanson, J.M. and Beard, B.B. (2012). Applying monte carlo simulation to launch vehicle design and requirements verification. *Journal of Spacecraft and Rockets*, 49(1), 136–144.

Hindi, H., Seong, C.Y., and Boyd, S. (2002). Computing optimal uncertainty models from frequency domain data. In *Proceedings of the 41st IEEE Conference on Decision and Control, 2002*. IEEE.

Hoblit, F.M. (1988). *Gust Loads on Aircraft: Concepts and Applications*. American Institute of Aeronautics and Astronautics.

Pfifer, H. and Seiler, P. (2016). Less conservative robustness analysis of linear parameter varying systems using integral quadratic constraints. *International Journal of Robust and Nonlinear Control*, 26(16), 3580–3594.

Seiler, P., Moore, R.M., Meissen, C., Arcak, M., and Packard, A. (2019). Finite horizon robustness analysis of LTV systems using integral quadratic constraints. *Automatica*, 100, 135–143.

Simplicio, P., Bennani, S., Lefort, X., .Marcos, A., and Roux, C. (2016). Structured singular value analysis of the vega launcher in atmospheric flight. *Journal of Guidance, Control, and Dynamics*, 39(6), pp. 1342–1355.

Veenman, J., Scherer, C.W., and Köroğlu, H. (2016). Robust stability and performance analysis based on integral quadratic constraints. *European Journal of Control*, 31, 1–32.

Wiesel, W.E. (2010). *Spaceflight dynamics*. Beavercreek, Ohio : Aphelion Press, 3rd ed edition.